

# <sup>1</sup> Contents

<b>2</b>	<b>1 Diamond detectors for radiation detection</b>	<b>2</b>
3	1.1 Semiconductor detectors . . . . .	3
4	1.2 Principles of signal formation in semiconductors . . . . .	4
5	1.2.1 Signal induction by moving charges . . . . .	5
6	1.2.2 Shockley-Ramo theorem . . . . .	7
7	1.2.3 Thermal excitation . . . . .	7
8	1.2.4 Space charge . . . . .	8
9	1.3 Carrier transport in a diamond sensor . . . . .	8
10	1.4 Radiation-induced current signals . . . . .	10
11	1.4.1 Mean energy loss . . . . .	11
12	1.4.2 Signal fluctuation . . . . .	11
13	1.4.3 Charge collection . . . . .	12
14	1.4.4 Charge trapping . . . . .	13
15	1.5 Radiation damage . . . . .	14
16	1.6 Temperature effects . . . . .	16
17	1.7 Electronics for signal processing . . . . .	16
18	1.7.1 Signal preamplifiers . . . . .	17
19	1.7.2 Analogue-to-digital converters . . . . .	19
20	1.7.3 Digital signal processing . . . . .	20

<sub>21</sub> **Chapter 1**

<sub>22</sub> **Diamond detectors for radiation  
23 detection**

<sub>24</sub> Diamond has been known for over two millennia, valued for its mechanical properties and  
<sub>25</sub> its appearance. When the procedures for its synthesis were discovered, diamond made its  
<sub>26</sub> way to a broad range of industries which exploit its optical and electrical properties. The  
<sub>27</sub> discovery of the Chemical Vapour Deposition (CVD, described below) as a new synthesis  
<sub>28</sub> process gave rise to a range of new applications. Purer specimens are used in electronics,  
<sub>29</sub> high-power switching devices, electrochemical systems, radiation sensors, quantum comput-  
<sub>30</sub> ing etc. Recently it was found that it also exhibits superconductivity [1]. This thesis focuses  
<sub>31</sub> on the use of diamond for radiation detection. An example of such a diamond sample is  
<sub>32</sub> shown in figure 1.1.

<sub>33</sub> Compared to a natural diamond, a CVD diamond used as a particle detector has almost  
<sub>34</sub> no impurities (foreign atoms like nitrogen or boron). If proper procedures are followed, the  
<sub>35</sub> diamond lattice can be grown very uniformly. This in turn improves electrical properties  
<sub>36</sub> of the grown sample. Such a diamond is an almost perfect thermal and electrical insulator.  
<sub>37</sub> However, its electrical behaviour is similar to that of a semiconductor. For this reason this  
<sub>38</sub> chapter first introduces semiconductor detectors and then describes the principle of signal  
<sub>39</sub> formation in semiconductors. Then it focuses on the diamond sensor and its properties.

<sub>40</sub> **Chemical vapour deposition** (CVD) [2] is a process where a material is deposited from  
<sub>41</sub> a gas onto a substrate, involving chemical reactions. It is often carried out under high  
<sub>42</sub> pressure and high temperatures. It takes place in enclosed chambers called furnaces with  
<sub>43</sub> careful regulation of the temperature, pressure and gas mixture. Synthetic diamond is  
<sub>44</sub> grown at 700–900 °C with a mixture of hydrogen and methane gas. At this temperature the  
<sub>45</sub> molecules dissociate into carbon and hydrogen atoms. The carbon atoms are the building  
<sub>46</sub> blocks and are deposited on the surface of the substrate.

<sub>47</sub> Under a carefully controlled pressure and temperature conditions with an added abrasive  
<sub>48</sub> atomic hydrogen the graphitic bonds break and form into diamond bonds. The speed of  
<sub>49</sub> the growth can be anywhere between 0.1 and 10 µm per hour. The detector grade samples  
<sub>50</sub> are grown at a rate of the order of 1 µm per hour. They can grow up to several millimetres  
<sub>51</sub> in thickness. The width of the samples, however, depends entirely on the substrate used.

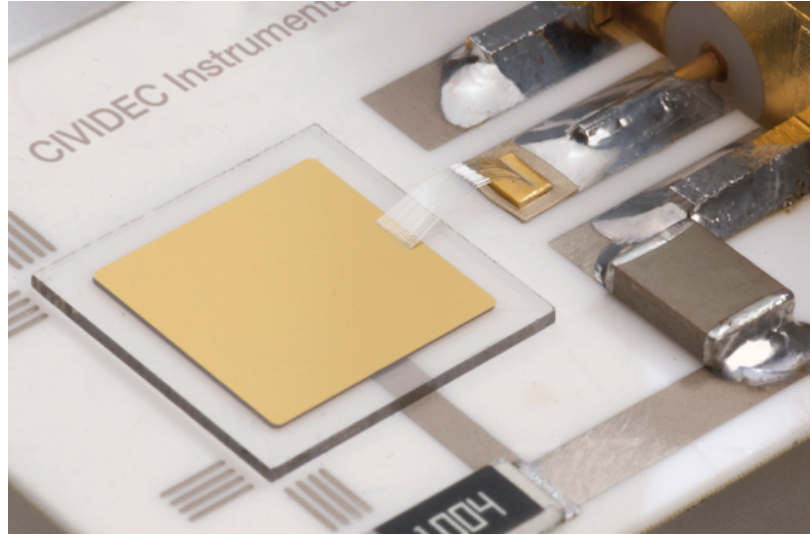


Figure 1.1: A pCVD diamond pad detector [3].

52 Diamond can be deposited on various materials: diamond, silicon, tungsten, quartz glass etc.  
53 The substrate material must be able to withstand the high temperatures during the CVD  
54 process. The diamond substrate does not need any surface pre-treatment. Carbon atoms  
55 form bonds with atoms in the existing crystal structure. This is the homo-epitaxial growth  
56 where the newly deposited atoms retain the orientation of the structure in the substrate.  
57 Other non-diamond substrates, however, need to be pre-treated, usually by being polished  
58 using diamond powder. Some powder particles remain on the surface, acting as seeds for  
59 the growth of small crystals or grains. These grains grow and at some point merge with the  
60 adjacent ones, making up a compact material. The lower side is later polished away. These  
61 diamonds are called *polycrystalline* (pCVD) whereas those grown on a diamond substrate  
62 are *single crystal* (sCVD) diamonds. The area of the former can be large - up to  $0.5 \text{ m}^2$  or  
63 more compact  $75 \text{ cm}^2$  in the case of detector grade diamonds, which can be further cut into  
64 smaller parts. The sCVD diamonds, on the other hand, can currently only achieve sizes up  
65 to  $1.5 \text{ cm}^2$ .

## 66 1.1 Semiconductor detectors

67 Semiconductor is a class of solids whose electrical conductivity is between that of a conductor  
68 and that of an insulator – of the order of  $10^{-5} \Omega^{-1} \text{ cm}^{-1}$ . Semiconductors consist of  
69 atoms with four electrons in their valence band, e.g. silicon–Si or germanium–Ge, or as  
70 combinations of two or more different materials, e.g. gallium arsenide–GaAs). The atoms  
71 in the lattice form valence bonds with adjacent atoms, creating solid crystal structures.

72 Semiconductor particle detectors are devices that use a semiconductor material to detect  
73 radiation. They work on the principle of an ionisation chamber. An incident particle ionises  
74 the atoms in the crystal lattice. The charges are freed if the deposited energy is higher than  
75 the energy band gap, i.e. the energy needed to excite an electron from its steady state  
76 to the conductance band. The freed charge carriers start drifting in an externally applied



Figure 1.2: The Insertable B-Layer – a silicon particle tracker installed in the ATLAS experiment in 2014 [5].

77 electric field, inducing current on the electrodes. The induced signal is amplified and read  
78 out by the electronics in the detector signal chain.

79 Semiconductor detectors are most widely used for tracking applications, like the In-  
80 sertable B-Layer shown in figure 1.2 [4], which was installed in ATLAS Experiment in 2014.  
81 First, they can be produced in thin layers to minimise the impact on the path of the inci-  
82 dent particles. Second, their low sensor capacitance allows for a fast signal response. Third,  
83 they are highly efficient and highly resistant to radiation damage. Finally, the industrial  
84 processes allow for a fine spatial segmentation, which in turn improves the track resolution  
85 of the detector systems.

86 Semiconductor sensors come in several configurations. The simplest type is a pad – a  
87 single plate with two electrodes. Pads are used for particle counting and radiation moni-  
88 toring. Next is a strip detector, a more finely segmented detector made out of long parallel  
89 sensing areas or strips. Normally each strip has its own signal line for readout. Usually the  
90 strip detectors are used in pairs – one detector is placed on top of the other at an angle to  
91 increase spatial resolution in both axes. The third and the most finely segmented is a pixel  
92 detector, consisting of a 2D array of independent sensing areas. In tracking applications,  
93 pixel detectors are used where the need for a high detection resolution and granularity re-  
94 quirement is the highest. Due to their high production cost and a high number of signal  
95 channels, they can only cover limited areas. Strip detectors can be used to cover larger  
96 areas in several consecutive layers.

## 97 1.2 Principles of signal formation in semiconductors

98 Particles can interact with the sensor in several ways, e.g. via bremsstrahlung [6], elastic  
99 or inelastic scattering or nuclear reactions [7]. Bremsstrahlung is radiation created when a  
100 particle is decelerated due to interaction with the electric field of the core of an atom. Elastic

101 scattering is deflection of the particle's trajectory due to the pull from the nucleus without  
 102 depositing any energy in it. This is in principle an unwanted effect in semiconductors as  
 103 it deteriorates the spatial resolution of the sensor. Inelastic scattering is the interaction  
 104 through which an electron in the atom is *ionised*. Nuclear reaction is the direct interaction  
 105 between the incident particle and the core of the atom. All these effects are competing  
 106 and are dependent on the particle's mass, momentum etc. The scope of this chapter is to  
 107 discuss the ionisation mechanism in semiconductors.

108 The energy of the electrons forming valence bonds between atoms in the crystal lattice  
 109 is within the *valence band* [8]. To break a bond and excite the electron into a *conduction*  
 110 *band*, a sufficient energy has to be applied. The minimal energy required is equal to the  
 111 energy band gap  $E_g$  of the semiconductor. Typical  $E_g$  values are 0.7 eV in Ge, 1.12 eV in  
 112 Si and 1.4 eV in GaAs. Diamond with its 5.5 eV band gap is considered an insulator. The  
 113 separation between the conductive and valence band is referred to as *forbidden gap* where  
 114 no electron states can exist.

115 An electron excited into the conduction band leaves behind a positively charged ion  
 116 with a vacancy – a hole – in its valence band, as shown in figure 1.3a. A free *electron-hole*  
 117 *pair* is thus created. The free electron travels through the crystal until it is recombined  
 118 with another hole. Similarly the positive charge of the hole attracts a bound electron in  
 119 the vicinity, causing it to break from the current bond and moving to the vacancy, thus  
 120 leaving behind a newly created hole. The process continues, making it look like the hole is  
 121 traveling through the material [8].

122 Both the electron and the hole are referred to as *charge carriers*. Without an externally  
 123 applied electrical field, they propagate in random directions. Therefore on average there is  
 124 no overall motion of charge carriers in any particular direction over time.

125 However, if an external electric field is applied to the crystalline structure, the free  
 126 electrons and holes drift toward the positive and negative potential, respectively, as shown  
 127 in figure 1.3b. While drifting, the charges couple with the electrodes, inducing current in  
 128 the circuit, which is explained by the Shockley–Ramo theorem below. Upon reaching the  
 129 electrodes the charges stop inducing the current. The equivalent electrical circuit is shown  
 130 in figure 1.3c.

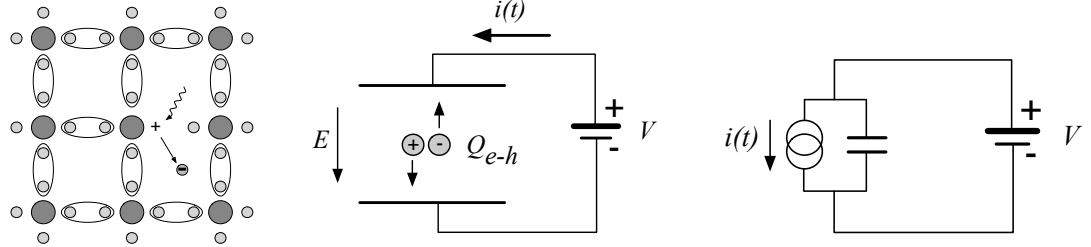
### 131 1.2.1 Signal induction by moving charges

132 The signal induction in a conducting plane by a point-like charge, which couples with  
 133 an electrode, is derived in [9]. The electrode can in this case be modelled as an infinite  
 134 conducting plane. When a point charge  $q$  is created (e.g. an electron-hole pair created  
 135 via ionisation), its electrostatic field lines immediately couple with the electrode, as seen  
 136 in figure 1.4a. The electric field on the metal surface due to a point-like charge  $q$  at the  
 137 distance  $z_0$  is

$$E_z(x, y) = \frac{q z_0}{2\pi\epsilon_0(x^2 + y^2 + z_0^2)^{\frac{3}{2}}} \quad E_y = E_z = 0. \quad (1.1)$$

138 A mirror charge appears on the conducting plane, with a charge density distribution

$$\sigma(x, y) = \epsilon_0 E_z(x, y) = \frac{q z_0}{2\pi(x^2 + y^2 + z_0^2)^{\frac{3}{2}}}. \quad (1.2)$$

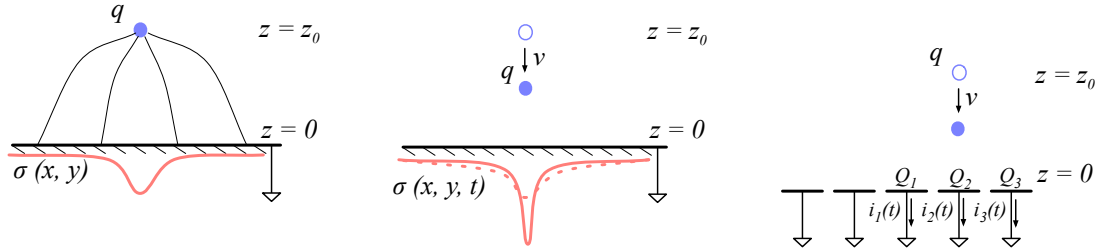


(a) Valence bonds in the crystalline structure can be broken, creating a free electron-hole pair

(b) The freed electron-hole pair starts drifting in the externally applied electric field. The electron and the hole both drift in the opposite directions towards the oppositely charged electrodes.

(c) Equivalent electrical circuit. The moving charges act as a current source.

Figure 1.3: In the equivalent electrical circuit diagram the electron-hole creation and drift can be modelled as a current source with a capacitor in parallel.



(a) Newly created point charge couples with the conductive plane.

(b) When the charge drifts, the charge density in the plane changes.

(c) The changing charge density in the small regions of the plane induces current.

Figure 1.4: A point-like charge inducing current in a conductive plane.

<sup>139</sup> The charge density integrated over the entire plane yields a mirror charge  $Q$ , which is an  
<sup>140</sup> opposite of point charge  $q$ :

$$Q = \int_{-\infty}^{\infty} \int_{-\infty}^{\infty} \sigma(x, y) dx dy = -q. \quad (1.3)$$

<sup>141</sup> The plane is then segmented into infinitely long strips with a width  $w$  whereby each of the  
<sup>142</sup> strips is grounded, as shown in figure 1.4c. Considering a charge density distribution 1.2, the  
<sup>143</sup> resulting mirror charge on a single strip  $Q_2$  directly below the point charge ( $x = 0, y = 0$ )  
<sup>144</sup> yields

$$Q_2(z_0) = \int_{-\infty}^{\infty} \int_{-w/2}^{w/2} \sigma(x, y) dx dy = -\frac{2q}{\pi} \arctan\left(\frac{w}{2z_0}\right) \quad (1.4)$$

<sup>145</sup> If the charge starts moving towards the conducting plane, the mirror charge density distribution  
<sup>146</sup> also changes, as shown in figure 1.4b. As a result the  $Q_2[z(t)]$  changes with time.  
<sup>147</sup> The changing charge is in effect an induced electric current  $i_2(t)$ :

$$i_2(t) = -\frac{d}{dt} Q_2[z(t)] = -\frac{\partial Q_2[z(t)]}{\partial z} \frac{\partial z(t)}{\partial t} = \frac{4qw}{\pi[4z(t)^2 + w^2]} v. \quad (1.5)$$

- 148 The movement of the point-like charge therefore induces current in the conducting plane.  
 149 The induced current is linearly dependent on the velocity of the point-like charge.

150 **1.2.2 Shockley-Ramo theorem**

151 W. Shockley [10] and S. Ramo [11] independently proposed a theory which explains how  
 152 a moving point charge induces current in a conductor. The Shockley-Ramo theorem can  
 153 therefore be used to calculate the instantaneous electric current induced by the charge  
 154 carrier or a group of charge carriers. It can be used for any number of electrodes. It states  
 155 that the current  $I_n^{\text{ind}}(t)$  induced on the grounded electrode  $n$  by a point charge  $q$  moving  
 156 along a trajectory  $\mathbf{x}(t)$  reads

$$I_n^{\text{ind}}(t) = -\frac{dQ_n(t)}{dt} = -\frac{q}{V_w} \nabla \Psi_n[\mathbf{x}(t)] v(t) = -\frac{q}{V_w} \mathbf{E}_n[\mathbf{x}(t)] v(t), \quad (1.6)$$

157 where  $\mathbf{E}_n(\mathbf{x})$  is the *weighting field* of electrode  $n$  in the case where the charge  $q$  is removed,  
 158 electrode  $n$  is set to voltage  $V_w = 1$  and all other electrodes are grounded. The weighting  
 159 field is defined as the spatial differential of the *weighting potential*:  $\mathbf{E}_n(\mathbf{x}) = \nabla \Psi_n(\mathbf{x})$ . In  
 160 the case of two parallel electrodes, the weighting field is  $E_w = -\frac{d\Psi}{dx} = -1/d$ , where  $d$  is the  
 161 distance between the electrodes. The resulting induced current is therefore

$$i(t) = \frac{q}{d} v_{\text{drift}}(x, t), \quad (1.7)$$

162 whereby  $v_{\text{drift}}$  is the drift velocity of the point-like charge and  $d$  is the distance between the  
 163 electrodes.  $d$  is defined by the dimensions of the sensor. The drift velocity is a function  
 164 of the externally applied electric field, as defined in section 1.3. If the electric field is set  
 165 to a constant value, the induced current is directly proportional to the drifting charge.  
 166 Therefore, by measuring the height of the induced current at a specific point of time the  
 167 number of moving charges can be deduced.

168 **1.2.3 Thermal excitation**

169 Electrons can be thermally excited to the conduction band. The intrinsic concentration of  
 170 thermally excited electrons  $n_i$  in semiconductors is proportional to[8]

$$n_i \propto \exp\left(-\frac{E_g}{2k_B T}\right) \quad (1.8)$$

171 wherein  $k_B = 1.381 \times 10^{-23} \text{ m}^2 \text{ kg s}^{-2} \text{ K}^{-1}$  is the Boltzmann constant,  $E_g$  is the energy  
 172 band gap of the semiconductor and  $T$  is the temperature in K. Due to the small band gap  
 173 in semiconductors a significant amount of electrons already occupies the conduction band  
 174 at room temperature due to thermal excitation, according to the probabilistic distribution.  
 175 To reduce this effect semiconductor sensors are doped with donors and acceptors, forming  
 176 a diode [8]. The diode is then inversely biased to deplete the material of all free charges.  
 177 Doped silicon fulfils most of the needs for particle physics requirements and is therefore  
 178 the most widely used material for particle detection. Diamond with its high energy band  
 179 gap on the other hand only has a negligible number of thermally excited electrons at room  
 180 temperature. Therefore a p-n junction is not needed, which simplifies the sensor production.

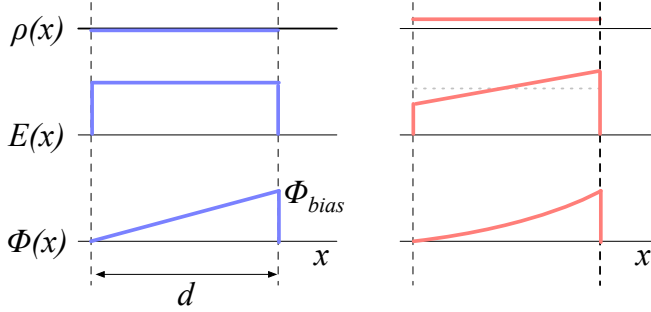


Figure 1.5: Left figure shows a profile of a diamond sensor only with an externally applied electric field. In the figure on the right a uniformly distributed space charge is added in the diamond, contributing to the internal electric field distribution. The induced current signal is proportional to the electrical field.  $d$  is the thickness of the diamond sensor.

<sup>181</sup> **1.2.4 Space charge**

<sup>182</sup> The Poisson equation shows that

$$\frac{d^2\Phi(x)}{dx^2} = \frac{dE(x)}{dx} = \frac{\rho(x)}{\epsilon} \quad (1.9)$$

<sup>183</sup> where  $\rho(x)$  is the space charge distribution,  $E$  is the electrical field and  $\Phi$  is the voltage  
<sup>184</sup> potential. In an ideal diamond, the externally applied high voltage potential on the two  
<sup>185</sup> electrodes decreases linearly through the sensor. The electrical field is therefore constant  
<sup>186</sup> throughout the sensor and the space charge distribution across it equals 0. However, space  
<sup>187</sup> charge may be introduced in the material either by means of accumulating of charge carriers  
<sup>188</sup> in the lattice (i.e. charge trapping) or already during sensor production. The space charge  
<sup>189</sup> can be either permanent or changing – sometimes it is possible to reduce it, as is shown  
<sup>190</sup> in chapter ???. All in all, it is very important to reduce it because it affects the shape of  
<sup>191</sup> the electrical signal. Since the drift velocity of the charge carriers is proportional to the  
<sup>192</sup> electrical field, the charges change their velocity while drifting through the space charge  
<sup>193</sup> region. Figure 1.5 compares the voltage potential, the electrical field and the space charge  
<sup>194</sup> for an ideal sensor as well as for that with a uniformly distributed positive space charge.

<sup>195</sup> **1.3 Carrier transport in a diamond sensor**

<sup>196</sup> This section describes the carrier transport phenomena in diamond. This theory provides  
<sup>197</sup> the basis for discussion about the measurements in chapter ???. Table 1.1 compares the  
<sup>198</sup> properties of diamond and silicon. Some of these values are revisited and used in the course  
<sup>199</sup> of this thesis.

Property	Diamond	Silicon
Band gap energy $E_g$ (eV)	5.5	1.12
Electron mobility $\mu_e$ ( $\text{cm}^2 \text{ V}^{-1} \text{ s}^{-1}$ )	1800 [12]	1500 [8]
Hole mobility $\mu_h$ ( $\text{cm}^2 \text{ V}^{-1} \text{ s}^{-1}$ )	2500 [12]	450 [8]
Breakdown field ( $\text{V cm}^{-1}$ )	$10^7$	$3 \times 10^5$
Resistivity ( $\Omega \text{ cm}$ )	$> 10^{11}$	$2.3 \times 10^5$
Intrinsic carrier density ( $\text{cm}^{-3}$ )	$< 10^3$	$1.5 \times 10^{10}$
Mass density ( $\text{g cm}^{-3}$ )	3.52	2.33
Atomic charge	6	14
Dielectric constant $\epsilon$	5.7	11.9
Displacement energy (eV/atom)	43	13 – 20
Energy to create an e-h pair (eV)	13	3.6
Radiation length (cm)	12.2	9.6
Avg. signal created/ $\mu\text{m}$ (e)	36	89

Table 1.1: Comparison diamond – silicon [8, 12].

When the charge carriers are freed in a semiconductor with no concentration gradient and without an externally applied electric field, they scatter in random directions with a thermal velocity  $v_{\text{th}}$  [8]. Their integral movement due to thermal excitation equals zero.

**Diffusion** is caused by the concentration gradient. In its presence the integral movement is in the direction of the lower concentration until an equilibrium is reached. The concentration profile dissolves with time forming a Gaussian distribution with variance  $\sigma(t) = \sqrt{Dt}$  [8] .

**Drift** is caused by an externally applied electrical field. In that case the carriers move along the field lines. In a sensor with a high applied field the diffusion contribution is negligible.

**Drift velocity**  $v_{\text{drift}}(E)$  is the speed at which the charge carriers drift through the diamond sensor [8].

**Mobility**  $\mu$  is a proportionality factor between the  $v_{\text{drift}}$  and the electric field  $E$  at low electric fields:  $v_{\text{drift}} = \mu E$ . Its units are in  $\text{cm}^2 \text{ V}^{-1} \text{ s}^{-1}$ .

**Phonon transport** is the transfer of energy of the moving charges to the lattice.

**Saturation velocity**  $v_{\text{sat}}^e$  is a velocity limit above which the carriers cannot reach. This is due to increasing phonon transport at a high electric field. The  $v_{\text{sat}}^e = v_{\text{sat}}^h = (14.23 \pm 0.12) \times 10^6 \text{ cm/s}$  for both positive and negative charge carriers has been derived from the measurements in [13].

The final equation for  $v_{\text{drift}}$  is therefore [14]

$$v_{\text{drift}}(E) = \mu(E)E = \frac{\mu_0 E}{1 + \frac{\mu_0 E}{v_{\text{sat}}}}. \quad (1.10)$$

It can be retrieved experimentally via the transit time measured with the Transient Current Technique (TCT). This technique enables the measurement of transit time  $t_t$  of the carriers through the sensor with the thickness  $d$ .

$$v_{\text{drift}}(E) = \frac{d}{t_t(E)}. \quad (1.11)$$

The velocities for holes and electrons usually differ. In diamond, the holes travel approximately 30 % faster than electrons at the room temperature [12].

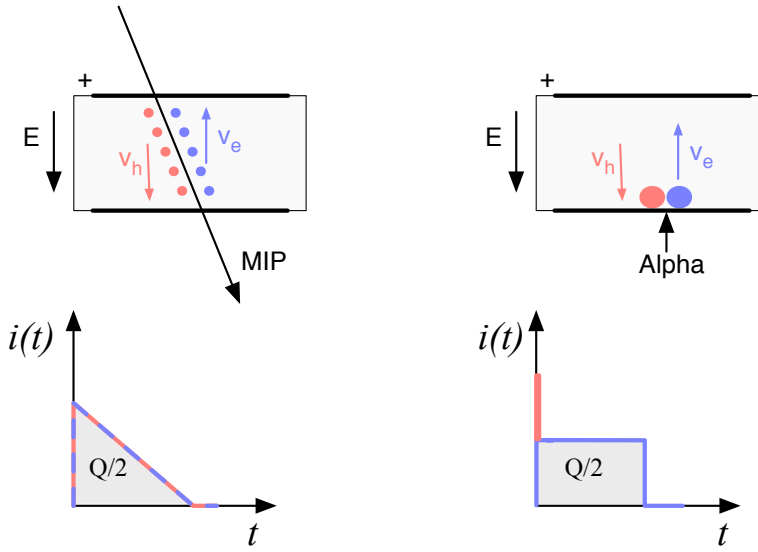


Figure 1.6: Charge carrier drift in diamond for  $\beta$  and for  $\alpha$  particles crossing the sensor at  $t = 0$ .

## 225 1.4 Radiation-induced current signals

226 When a highly-energetic particle travels through the sensor, it interacts with atoms in the  
 227 lattice. It ionises the valence electrons, creating electron-hole (e-h) pairs on its way. It can  
 228 either deposit only a fraction of its energy and exit the sensor on the other side or it can get  
 229 stopped in the sensor, depositing all of its energy. A special case is when it interacts with the  
 230 core of the atom in the middle of the sensor by means of a nuclear interaction. All these  
 231 various types interactions produce different amounts and different spatial distributions of  
 232 e-h pairs.

233 The two most frequent types are shown in figure 1.6. The first figure shows the inter-  
 234 action of an incident MIP. The electrons and holes created all along the trajectory of the  
 235 particle immediately start drifting towards the positive and negative electrode, respectively.  
 236 At  $t = 0$  all charges drift, contributing to the maximum induced current. Those closest to  
 237 the electrodes have a very short drift path. They stop inducing current upon reaching the  
 238 electrode. The resulting current signal is a triangular pulse with a sharp rising edge and a  
 239 linear falling edge. Gradually all the charge carriers reach the electrode. The accumulated  
 240 charge  $Q_s$  equals to the sum of the contributions of the positive and negative charge carriers.

241 The second type of interaction happens when the particle is stopped in the diamond  
 242 close to the point of entry. Most of its energy is deposited in a small volume close to the  
 243 electrode. A cloud of charge carriers is created and the charges with the shorter path to the  
 244 electrode disappear almost instantly. The carriers of the opposite charge, however, start  
 245 drifting through the sensor to the other electrode. In an ideal diamond sensor, their velocity  
 246 is constant throughout the drift up until they are collected at the opposite electrode. The  
 247 contribution of the first charge cloud is a peak with a short time. The cloud drifting through

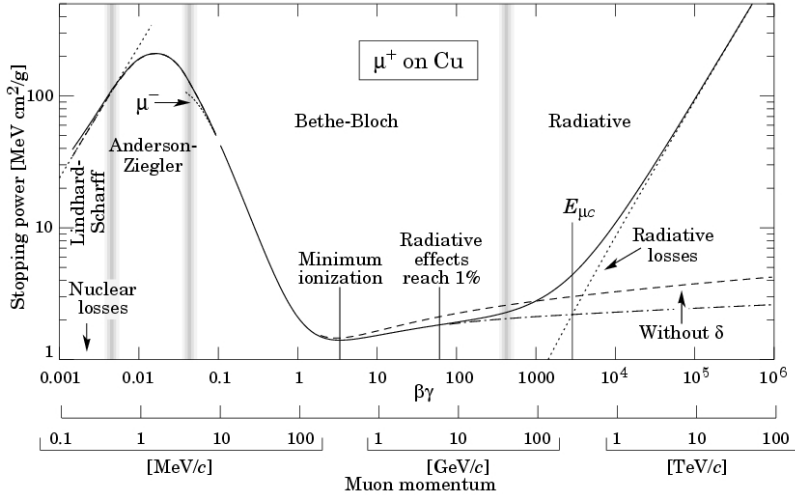


Figure 1.7: Stopping power for muons according to the Bethe-Bloch formula [15].

248 the sensor, on the other hand, induces a current signal with a flat top. The resulting signal  
249 has a shape of a rectangle, with a spike in the beginning. The accumulated charge  $Q_s$  is  
250 equal to a half of the deposited charge by the stopped particle.

251 The two aforementioned types of interactions have well defined signal responses. Nuclear  
252 interactions on the other hand yield various results. The resulting signal shape depends on  
253 the decay products of the interaction, which can be  $\alpha$ ,  $\beta$  or  $\gamma$  quanta or other nuclei,  
254 inducing a mixed shaped signal.

#### 255 1.4.1 Mean energy loss

256 A mean energy loss of a particle traversing the detector as a function of the momentum is  
257 given with the Bethe-Bloch equation [15]:

$$-\left\langle \frac{dE}{dx} \right\rangle = \frac{4\pi}{m_e c^2} \cdot \frac{nz^2}{\beta^2} \cdot \left( \frac{e^2}{4\pi\epsilon_0} \right)^2 \cdot \left( \ln \left( \frac{2m_e c^2 \beta^2}{I \cdot (1 - \beta^2)} \right) - \beta^2 \right) \quad (1.12)$$

258 The resulting function for a muon is shown in figure 1.7. At a momentum of around  
259 300 MeV/c the incident particle deposits the lowest amount of energy. Hence it is referred  
260 to as the *minimum ionising particle* or a MIP.

#### 261 1.4.2 Signal fluctuation

262 Two important sensor properties are the magnitude of the signal and the fluctuations of  
263 the signal at a given absorbed energy. They determine the relative resolution  $\Delta E/E$ . For  
264 semiconductors the signal fluctuations are smaller than the simple statistical standard de-  
265 viation  $\sigma_Q = \sqrt{N_Q}$ . Here  $N_Q$  is the number of released charge pairs, i.e. the ratio between  
266 the total deposited energy  $E_0$  and the average energy deposition  $E_i$  required to produce an  
267 electron-hole pair. [16] shows that the standard deviation is  $\sigma_Q = \sqrt{F N_Q}$ , where  $F$  is the

## 1.4. RADIATION-INDUCED CURRENT SIGNALS

---

268 Fano factor [16] (0.08 for diamond and 0.115 for silicon [17]). Thus, the standard deviation  
269 of the signal charge is smaller than expected,  $\sigma_Q \approx 0.3\sqrt{N_Q}$ . The resulting intrinsic  
270 resolution of semiconductor detectors is

$$\Delta E_{\text{FWHM}} = 2.35\sqrt{FEE_i} \quad (1.13)$$

271 wherein  $E_i(Si) = 3.6$  eV and  $E_i(Di) = 13$  eV. E.g., for an  $\alpha$  particle with energy  $E_\alpha = 5.5$   
272 MeV the calculated resolution in diamond is equal to  $\Delta E_{\text{FWHM}} = 5.6$  keV. This defines the  
273 minimum achievable resolution for energy spectroscopy with semiconductors.

### 274 1.4.3 Charge collection

275 The total measured charge  $Q_i$  is the integral of the induced current:

$$Q_i = \int i_{\text{ind}}(t)dt. \quad (1.14)$$

276 The expected charge  $Q_0$  can be calculated using the thickness of the sensor  $d$  and the  
277 average number of e-h pairs created per  $\mu\text{m}$   $\delta_d$ , which is 36 e-h/ $\mu\text{m}$  for diamond according  
278 to table 1.1. The expected charge created by a MIP flying through a sensor with a thickness  
279  $d = 500$   $\mu\text{m}$  perpendicular to the electrodes is

$$Q_{\text{MIP}} = \delta_d \cdot d \cdot q = 18 \times 10^3 \text{ eh} \cdot q = 2.9 \text{ fC} \quad (1.15)$$

280 where  $q = 1.6 \times 10^{-19}$  C is the elementary charge. If a particle stops in the sensor, it  
281 deposits all its energy. In this case the number of created e-h pairs is calculated according  
282 to equation 1.16 using  $E_{\text{eh}}$ , the energy required to create an e-h pair. For diamond this  
283 value is 13, according to table 1.1. For a 5.5 MeV  $\alpha$  particle emitted from an  $^{241}\text{Am}$  source  
284 the expected charge is

$$Q_\alpha = \frac{E}{E_{\text{e-h}}} \cdot q = \frac{5.5 \text{ MeV}}{13 \text{ eV}} \cdot q = 4.25 \times 10^5 \text{ eh} \cdot q = 68 \text{ fC}. \quad (1.16)$$

285 where  $E$  is the energy of the incident particle, which is almost for a factor of 24 larger than  
286 expected charge of a MIP. The charge collection efficiency (CCE) is the ratio between the  
287 measured and expected charge:

$$CCE = \frac{Q_i}{Q_0} = \frac{Q_i}{\delta_d \cdot d} \cdot 100\%. \quad (1.17)$$

288 The charge collection distance (CCD) is a measure of an average path that the charge  
289 carriers travel before getting trapped:

$$CCD = \frac{Q_i}{\delta_d} \quad (1.18)$$

290 and is usually given in units of  $\mu\text{m}$ .

291 Carriers that get trapped stop contributing to the overall induced current on the elec-  
292 trodes. The more charges are trapped along their drift path, the more the current induced  
293 on the electrodes is decreased. This in turn yields a lower integrated charge. An expected

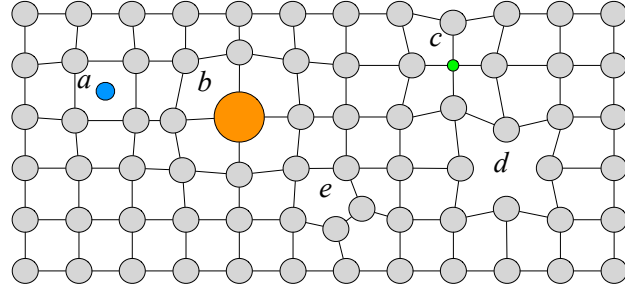


Figure 1.8: Impurities and non-uniformities in the crystal lattice due to radiation damage.

294 CCE for non-irradiated sCVD diamonds is close to 100 %. For highest quality non-irradiated  
 295 pCVD diamonds it ranges between 40 % and 60 %. In other words, high-quality pCVD  
 296 diamonds already have traps introduced by means of grain boundaries, which are created in  
 297 the growing process. Traps can also be created by damaging the diamond using radiation  
 298 (discussed in section 1.5). The more the sensor is irradiated, the larger number of traps is  
 299 introduced in the material and the higher is the probability that the carriers are stopped  
 300 on the way, reducing in turn the integrated charge. Therefore the CCD and CCE can be  
 301 used as a means to quantify the detector damage due to radiation.

#### 302 1.4.4 Charge trapping

303 Various types of lattice defects can be created in diamond, similar to those in silicon [18].  
 304 Figure 1.8 shows several examples of lattice damage:

- 305     a) foreign interstitial (e.g. H, Li),
- 306     b, c) foreign substitutional (e.g. N, P, B),
- 307     d) vacancy and
- 308     e) self interstitial.

309 These non-uniformities form new energy levels in the forbidden gap. These intermediate  
 310 levels are referred to as charge traps because they can trap moving charge carriers. The  
 311 energy level of the trapped carriers is reduced from the conduction band to the energy level of  
 312 the trap. Different types of lattice damage have different energy levels. The carriers trapped  
 313 in a shallow trap – an energy level close to the conduction band – have a high probability  
 314 of being thermally excited back into the conduction band whereby they continue drifting  
 315 towards the electrode. Their activation energy is therefore low. Those trapped in a deep  
 316 trap close to the middle of the forbidden gap need a much higher activation energy, which  
 317 in turn increases the average time to their release due to thermal excitation.

318 The energy band jumping goes the other way, too. The carriers in the valence band may  
 319 use the intermediate energy levels as “stepping stones” to jump to the conduction band and  
 320 start drifting in the externally applied electric field. These intermediate energy levels are  
 321 referred to as the generation centres of leakage current.

322 The charge carriers that drift through the bulk get stopped in the charge traps with a  
 323 certain probability. This trapping happens uniformly throughout the diamond. In other  
 324 words, the number of carriers in the moving charge cloud is gradually reduced. This in turn  
 325 reduces the induced current. The number of drifting carriers per unit of length follows a  
 326 decaying exponential function

$$I(t) = I_0 + I(0) \cdot e^{-\frac{t-t_0}{\tau}}, \quad (1.19)$$

327 where  $I(0)$  is the initial induced current,  $I_0$  is the end current,  $t$  is time,  $t_0$  is temporal  
 328 displacement of the pulse and  $\tau$  is the decay time constant. This value describes how long  
 329 it takes before the amplitude of the pulse decreases to 63 % of its initial height.

330 **Priming/pumping**

331 Priming or pumping [19] is a process of irradiating the diamond with ionising radiation  
 332 with a goal to improve the sensor properties. The pumping process strongly reduces the  
 333 concentration of active carrier trapping centres. This leads to an enhancement of electronic  
 334 properties of such material. The improved transport properties due to a reduced number  
 335 of active charge traps give rise to an increased charge collection efficiency. The diamond is  
 336 usually pumped for a few hours using a strong  $\beta$  source, preferably a  $^{90}\text{Sr}$  source with the  
 337 activity of at least 50 MBq. The diamond remains in a pumped state from a few minutes  
 338 to several days, depending on the quality of the material. A direct exposure to light results  
 339 in an immediate return to an non-pumped state.

340 **1.5 Radiation damage**

341 Exposure to ionising radiation degrades sensors by deforming the crystal lattice and intro-  
 342 ducing charge traps in the material.

343 Radiation damage varies with the type of radiation and its energy. There are several  
 344 models existing [20, 21] that try to explain the impact of irradiation and to provide *damage*  
 345 *factors* to compare the radiation damage between different particles. The standard way is  
 346 to convert the damage into *1 MeV neutron equivalent fluence* [22]. Some models have been  
 347 extensively verified with simulations and with experiments. In these experiments the charge  
 348 collection in sensors is measured before and after irradiation. This procedure is repeated  
 349 several times, with a measurement point taken after every irradiation. Then the charge  
 350 collection for this set of measurements is plotted as a function of the radiation dose received  
 351 by a specific particle at a specific energy. From this a damage factor  $k_\lambda$  can be extracted.  
 352 Damage factors have to be measured across a range of energies and types of radiation to  
 353 properly quantify the damage in the sensors. Finally they are compared to the simulations  
 354 to validate the theoretical models.

355 Diamond is an expensive material and the technology is relatively new as compared to  
 356 silicon. Therefore few institutes are carrying out diamond irradiation studies. To join the  
 357 efforts, the RD42 collaboration [23] has been formed. It gathers the experimental data from  
 358 diamond irradiation studies. Unlike with silicon, the experimental results so far show no  
 359 significant correlation with the NIEL (non-ionising energy loss) model [20], which correlates

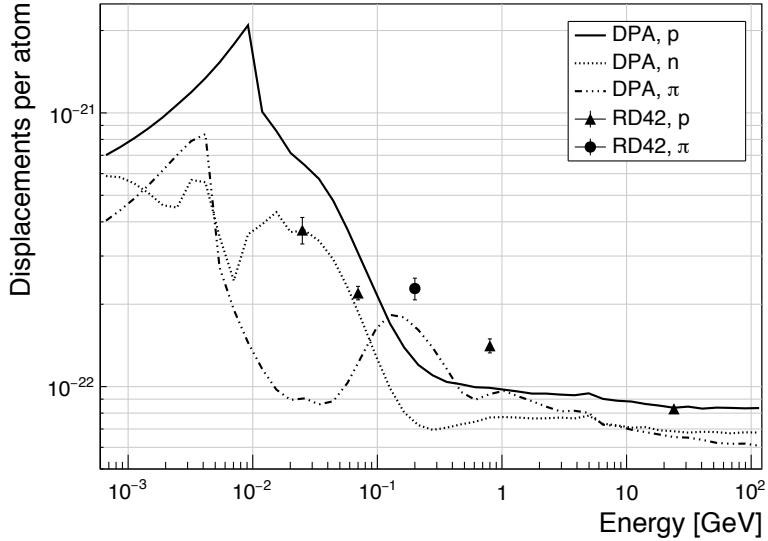


Figure 1.9: Diamond radiation damage - a model based on displacements per atom [21]. The figure shows the DPA as a function of the kinetic energy for protons, neutrons and pions. Added are data points for protons and pions by RD42 [24].

detector efficiency with the number of lattice displacements. Therefore an alternative model was proposed [21], correlating the diamond efficiency with the number of displacements per atom (DPA) in the material. The idea is that if the recoil energy of an incident particle is higher than the lattice binding energy (42 eV for diamond), the atom is displaced from its original position. The newly formed vacancy acts as a trap for drifting charge carriers. The more displacements that form in the crystal, the higher is the probability that a drifting carrier gets trapped. However, different types of particles interact differently with the material. In addition the mechanisms of interaction at low energies are different to those at high energies. To assess the damage for individual particles at a range of energies, simulations need to be run first. The simulation shown in [21] shows the DPA model for a range of energies of proton, pion and neutron irradiation in diamond. Figure 1.9 contains the simulation results as well as the superimposed empirical results of several irradiation studies. According to the figure, a 300 MeV pion beam damages the diamond material twice as much as a 24 GeV proton beam. The data points obtained by RD42 are also added to the figure. They have been normalised to damage by 24 GeV protons. This value has been chosen because radiation damage at this energy and radiation type is well understood at CERN.

### 377 Irradiation damage factor

378 The irradiation damage factor  $k_\lambda$  is a means to quantify irradiation damage of a specific  
 379 type of radiation at a specific energy. Via this factor different types of irradiation can be  
 380 compared. It is obtained experimentally by measuring the CCD of a number of samples at  
 381 various irradiation steps and fitting the equation 1.20 to the data.  $\lambda$  is the measured CCD,

## 1.6. TEMPERATURE EFFECTS

---

<sup>382</sup>  $\lambda_0$  is the CCD of a non-irradiated sample and  $\Phi$  the radiation dose. As a reference, the  
<sup>383</sup> damage factor for 24 GeV protons is set to  $1 \times 10^{-18} \mu\text{m}^{-1} \text{cm}^{-2}$ .

$$\frac{1}{\lambda} = \frac{1}{\lambda_0} + k_\lambda \cdot \Phi \quad (1.20)$$

## <sup>384</sup> 1.6 Temperature effects

<sup>385</sup> The band gap energy in diamond is equal to  $E_g = 5.5 \text{ eV}$  while the average energy to produce  
<sup>386</sup> an electron-hole pair is  $E_{e-h} = 13 \text{ eV}$ . This means there is excessive energy deposited in  
<sup>387</sup> the diamond bulk. An incident  $\alpha$ -particle stops within  $\sim 10\text{--}15 \mu\text{m}$  of the bulk, transferring  
<sup>388</sup> all its energy to the lattice during deceleration. A part of this energy directly ionises the  
<sup>389</sup> carbon atoms, creating free electron-hole pairs.

<sup>390</sup> The remaining energy, however, is converted into lattice vibrations – phonons [25, 12]. In  
<sup>391</sup> other words, the lattice within the ionisation volume of approximately  $\sim 15 \mu\text{m} \times \sim 2 \text{ nm}$  [12]  
<sup>392</sup> is briefly heated up. The hot plasma then cools down to the temperature of the surrounding  
<sup>393</sup> material by means of heat dissipation, i.e. phonon transport.

<sup>394</sup> The free electron binds with the free hole into a bound state (not recombination) –  
<sup>395</sup> the exciton [26]. The exciton binding energy is 80 meV, which introduces an energy level  
<sup>396</sup> within the forbidden gap just under the conduction band. At higher temperatures the  
<sup>397</sup> lattice provides enough energy to thermally excite the electron from the exciton state back  
<sup>398</sup> to the conduction band. At lower temperatures, however, the exciton lifetime increases,  
<sup>399</sup> which means that it takes a longer time for the electrons to get re-excited to the conduction  
<sup>400</sup> band. The re-excitation lifetime at room temperature is  $\sim 30 \text{ ps}$ , increasing to  $\sim 150 \mu\text{s}$  at  
<sup>401</sup> 50 K [12]. This means that some of the bound electrons do not even start drifting within  
<sup>402</sup> the period of  $\sim 10 \text{ ns}$ , which is the expected carrier drift time. When they are finally freed,  
<sup>403</sup> the current they induce is already hidden in the electronics noise. The effective area of the  
<sup>404</sup> observed current pulse is therefore smaller than that of a pulse induced by all the carriers  
<sup>405</sup> drifting at the same time. This in effect reduces the measured collected charge. The longer  
<sup>406</sup> the time constant, the lower the measured collected charge, as shown in section 1.6.

### <sup>407</sup> Collected charge as a function of temperature

<sup>408</sup> The area below the current pulse is proportional to the charge collected by the diamond  
<sup>409</sup> detector. The collected charge is measured as a function of temperature. First, the ampli-  
<sup>410</sup> tude values of the averaged pulses at a bias voltage of  $\pm 500 \text{ V}$  and across the temperature  
<sup>411</sup> range between 4 K and 295 K have to be integrated. Then a calibration factor is used to  
<sup>412</sup> derive the charge for all data points. The results of such measurements have been presented  
<sup>413</sup> in [12]. Chapter ?? shows the results of the measurements taken in the scope of this thesis.

## <sup>414</sup> 1.7 Electronics for signal processing

<sup>415</sup> This section describes the electronics of a detector, starting with a description of signal  
<sup>416</sup> amplifiers and then discussing the digitisation and signal processing. All these stages are

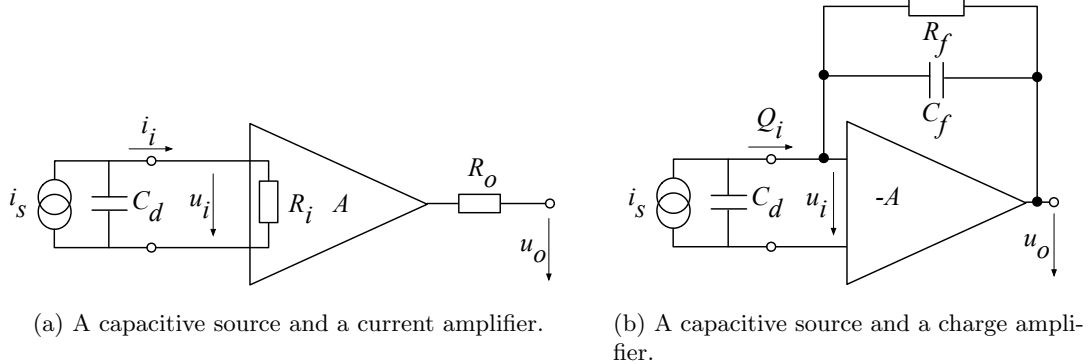


Figure 1.10: Simplified equivalent circuits of a current and charge amplifier.

417 necessary to extract information from the sensor. First, the signal has to be amplified.  
 418 Then it is digitised and finally processed in a specially designed processor or a logic unit.

### 419 1.7.1 Signal preamplifiers

420 The signal charge generated in the sensor by a single energetic particle is of the order of a few  
 421 fC. The range of the induced current for single particles is typically between  $10^{-8}$  A ( $\beta, \gamma$   
 422 radiation) and  $3 \times 10^{-7}$  A ( $\alpha$  radiation). Signals as low as these have to be pre-amplified  
 423 before processing. Depending on the measurement, several types of signal amplifiers can  
 424 be used. The preamplifiers are designed to minimise electronic noise while maximising  
 425 gain, thus maximising the signal-to-noise ratio (SNR). In addition, a bandwidth limit must  
 426 be optimised to minimise the information loss due to signal shape deformation. A critical  
 427 parameter is the total capacitance, i.e. the sensor capacitance together with the capacitance  
 428 load of the preamplifier. The SNR improves with a lower capacitance. Several types of  
 429 amplifiers can be used, all of which affect the measured pulse shape. Two preamplifiers are  
 430 used most commonly, a current and a charge sensitive amplifier. Both are described below.

#### 431 Current amplifier

432 Figure 1.10a shows the equivalent circuit of a current source and a current amplifier. An  
 433 amplifier operates in current mode if the source has a low charge collection time  $t_c$  with re-  
 434 spect to the  $R_i C_d$  time constant of the circuit. In this case the sensor capacitance discharges  
 435 rapidly and the output current  $i_o$  is proportional to the instantaneous current  $i_i$ . The am-  
 436 plifier is providing a voltage gain, so the output signal voltage  $u_o$  is directly proportional  
 437 to the input voltage  $u_i$ :

$$u_o(t) = A \cdot R_i \cdot i_s(t). \quad (1.21)$$

438 The detector capacitance  $C_d$  together with the input resistance of the amplifier  $R_i$  defines  
 439 the time constant of the signal, as shown in figure 1.11. The higher  $C_d$ , the slower is the  
 440 response of the amplifier. For the case of the diamond sensor, which has the capacitance of  
 441 the order of 2 pF and the input resistance of 50  $\Omega$ , the resulting time constant is  $\tau = 10^{-10}$  s.  
 442 This yields the signal rise time  $t_r \sim 2.2\tau = 2.2 \times 10^{-10}$  s.

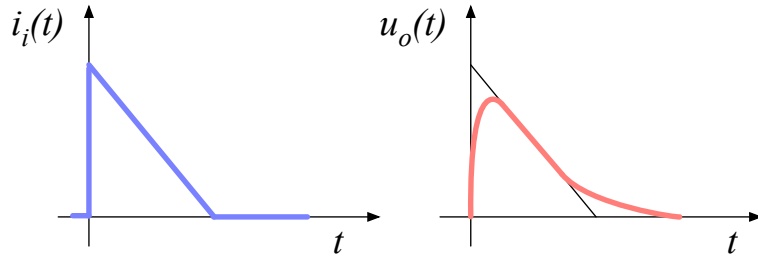


Figure 1.11: Input and output signal of the current amplifier.

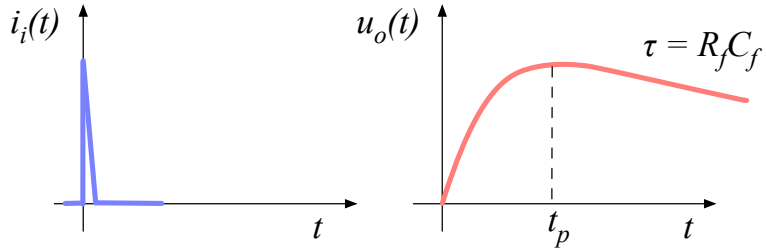


Figure 1.12: Input and output signal of the charge amplifier.

#### <sup>443</sup> Charge-sensitive amplifier

<sup>444</sup> In order to measure integrated charge in the sensor, a feedback loop is added to the amplifier,  
<sup>445</sup> as shown in figure 1.10b. The feedback can be used to control the gain and input resistance,  
<sup>446</sup> as well as to integrate the input signal. The charge amplifier is in principle an inverting  
<sup>447</sup> voltage amplifier with a high input resistance.

<sup>448</sup> In an ideal amplifier the output voltage  $u_o$  equals  $-Au_i$ . Therefore the voltage difference  
<sup>449</sup> across the capacitor  $C_f$  is  $u_f = (A + 1)u_i$  and the charge deposited on the capacitor is  
<sup>450</sup>  $Q_f = C_f u_f = C_f(A + 1)u_i$ . Since no current can flow into the amplifier, all of the signal  
<sup>451</sup> current must charge up the feedback capacitance, so  $Q_f = Q_i$ .

<sup>452</sup> In reality, however, charge-sensitive amplifiers respond much slower than is the duration  
<sup>453</sup> of the current pulse from the sensor. In addition, a resistor is added to the feedback line in  
<sup>454</sup> parallel to the capacitor. The resistor and capacitor define the decay time constant of the  
<sup>455</sup> pulse, as shown in figure 1.12. This is necessary to return the signal to its initial state to  
<sup>456</sup> be ready for a new measurement.

#### <sup>457</sup> Analogue electronic noise

<sup>458</sup> The electronic noise determines the ability of a system to distinguish different signal levels.  
<sup>459</sup> The analogue signal contains ample information about the type and energy of incident  
<sup>460</sup> radiation, which can quickly be erased or altered if the signal properties change. Therefore  
<sup>461</sup> the noise contributions to the signal must be well understood to qualify the information

462 the signal is carrying. The important contributions are listed below. Thermal or Johnson–  
 463 Nyquist noise [27, 28] is the dominant noise contribution in the use case for diamond detector  
 464 signal amplification and therefore defines the limitations of the detector system. This noise  
 465 type is generated by the random thermal motion of charge carriers. The frequency range  
 466 of the thermal noise is from 0 to  $\infty$  with a predominantly uniform distribution. Therefore  
 467 this is nearly a white noise. The resulting signal amplitude has a Gaussian distribution.  
 468 The RMS of the open-loop equivalent voltage is defined as

$$u_{\text{RMS}} = \sqrt{4k_B RT \Delta f} \quad (1.22)$$

469 where  $k_B$  is the Boltzmann constant,  $R$  is the input resistance of the amplifier,  $T$  its tem-  
 470 perature and  $\Delta f$  the frequency range. This equation shows that it is possible to reduce the  
 471 noise RMS by either (1) reducing the frequency range, (2) reducing the resistance or (3)  
 472 reducing the temperature.

473 Contributions of shot noise, flicker noise and burst noise and other types are not sig-  
 474 nificant relative to the thermal noise. However, the contributions of external factors can  
 475 severely deteriorate the signal. This means the noise produced by capacitive or inductive  
 476 coupling with an external source, which causes interference in the signal. These effects can  
 477 be reduced by shielding the electronics and avoiding ground loops.

### 478 1.7.2 Analogue-to-digital converters

479 An analogue-to-digital converter (ADC) is a device that converts the analogue electrical  
 480 signal on the input to its digital representation - a series of digital values. This involves a  
 481 quantisation – *sampling* of the signal at a defined sampling period, resulting in a sequence  
 482 of samples at a discrete time period and with discrete amplitude values. The resolution  
 483 of the ADC is the number of output levels the ADC can quantise to and is expressed in  
 484 bits. For instance, an ADC with a resolution equal to  $n = 8$  bit has a dynamic range of  
 485  $N = 2^n = 256$  steps. The resulting voltage resolution  $Q_{\text{ADC}}$  at the input voltage range of  
 486  $V_{\text{ADC}} = \pm 50$  mV is then

$$Q_{\text{ADC}} = \frac{V_{\text{ADC}}}{2^n} = \frac{100 \text{ mV}}{2^8 \text{ bit}} = 0.39 \text{ mV/bit.} \quad (1.23)$$

487 With a sampling period of  $t_s = 1$  ns the sampling rate is  $f_s = 1$  GS/s (gigasample per second).  
 488

**Quantisation error and quantisation noise** (or a round-off error) is a contribution to the overall measurement error due to digitisation (rounding). The quantisation error is defined as a difference between the actual analog value and the closest digitised representation of this value, therefore by the least significant bit (LSB), as seen in figure 1.13. The input signal amplitude is typically much larger than the voltage resolution. In this case the quantisation error is not directly correlated with the signal and has an approximately uniform distribution. The probability density function  $P(x)$  therefore has a rectangular shape bounded by  $(-\frac{1}{2}\text{LSB}, \frac{1}{2}\text{LSB})$ :

$$P(x) = \begin{cases} \frac{1}{\text{LSB}}, & -\frac{1}{2}\text{LSB} \leq x \leq \frac{1}{2}\text{LSB} \\ 0, & \text{otherwise.} \end{cases} \quad (1.24)$$

$$(1.25)$$

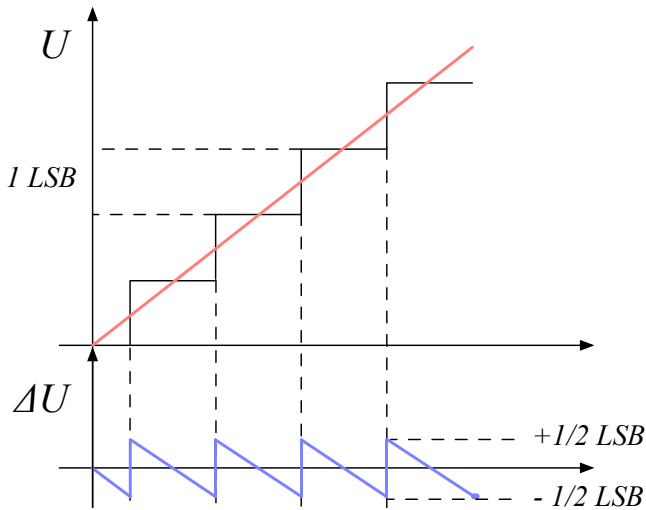


Figure 1.13: Input signal digitisation and quantisation error.

489 The height equal to  $\frac{1}{\text{LSB}}$  preserves the integrated probability of 1. The variance of the  
490 distribution is

$$\sigma^2 = \int P(x)(x - \mu)^2 dx. \quad (1.26)$$

491 The population mean is  $\mu = 0$ , therefore

$$\sigma^2 = \int_{-\frac{1}{2}\text{LSB}}^{\frac{1}{2}\text{LSB}} \frac{1}{\text{LSB}} x^2 dx = \frac{x^3}{3\text{LSB}} \Big|_{-\frac{1}{2}\text{LSB}}^{\frac{1}{2}\text{LSB}} = \frac{\text{LSB}^2}{12}. \quad (1.27)$$

492 The RMS of the quantisation noise is defined as the square root of the variance:

$$\Delta Q_{\text{ADC}} = \sqrt{\sigma^2} = \frac{1}{\sqrt{12}} \text{LSB} \sim 0.289 \text{ LSB}. \quad (1.28)$$

493 For the example above the quantisation error equals  $\Delta Q_{\text{ADC}} = 0.11 \text{ mV}$ . The error depends  
494 strongly on the linearity of the ADC, but this is out of scope of this document as the devices  
495 used have ADCs with a very good linearity.

### 496 1.7.3 Digital signal processing

497 The digitised signal can be processed to extract useful information. Therefore after the  
498 signal amplification and digitisation the signal is routed in a device which handles the  
499 digital analysis. The signal can either be processed immediately (in real time) or it can be  
500 saved to a data storage for analysis at a later stage (offline). The devices carrying out the  
501 processing can be multipurpose (e.g. Field Programmable Gate Arrays) or dedicated (e.g.  
502 Application-Specific Integrated Circuits).

503 **Field Programmable Gate Array** (FPGA) is an integrated circuit designed to be re-  
504 programmable and reconfigured after manufacturing. It consists of a set of logic gates that

505 can be interconnected in numerous combinations to carry out a set of logic operations.  
506 Many such logic operations can take place in parallel, making the FPGA a powerful tool  
507 for signal processing. FPGAs are often used during system development or in systems in  
508 which the requirements might change with time. They can be reprogrammed in the order of  
509 seconds. In addition, the logic design only needs minor changes when migrating to a newer  
510 version of the FPGA chip of the same vendor. The FPGAs also offer faster time-to-market  
511 with comparison to application-specific solutions, which have to be developed. On the other  
512 hand, the price per part can be significantly higher than for the application-specific solu-  
513 tions. Also, their other major disadvantages are a high power consumption and a relatively  
514 low speed as compared to more application-specific solutions. However, today's solutions  
515 are capable of clock speeds higher than 500 MHz. Together with the integrated digital  
516 signal processing blocks, embedded processors and other modules, they are already very  
517 powerful and versatile. All in all, FPGAs are a good choice for prototyping and limited  
518 production, for projects with limited requirements for speed and complexity.

519 **Application-Specific Integrated Circuit** (ASIC) is an integrated circuit designed for  
520 a specific use. The design cannot be modified after chip production, as is the case with  
521 FPGAs. On the other hand, the ASICs can be optimised to perform a required operation  
522 at a high speed and at a low power consumption. In addition, due to the specific design the  
523 size of the chip can be much smaller. ASICs can be designed as hybrid chips, containing  
524 both a digital and an analog part. Finally, ASICs can be designed to withstand much higher  
525 irradiation doses than FPGAs and can therefore be used in harsh environments like in space  
526 or in particle colliders.

527 To update the chip, the design has to be submitted to a foundry, which produces the new  
528 chips with a turnover time of 4—6 weeks. The costs of a submission are high, but the  
529 price per part can be reduced significantly with a high volume. To sum up, ASICs are used  
530 for high volume designs with well defined requirements where some stringent constraints in  
531 terms of power consumption and speed have to be met.

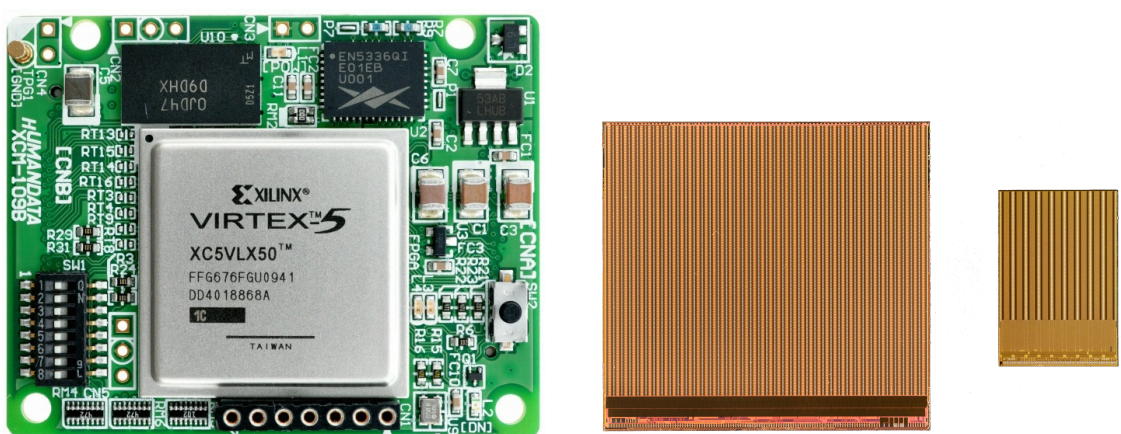


Figure 1.14: An example of a Xilinx Virtex 5 FPGA [29] and an FE-I4 and FE-I3 ASIC chip [30].

# <sup>532</sup> Bibliography

- <sup>533</sup> [1] E. A. Ekimov, V. A. Sidorov, E. D. Bauer, N. N. Mel'nik, N. J. Curro, J. D. Thompson,  
<sup>534</sup> and S. M. Stishov. Superconductivity in diamond. *Nature*, 428(6982):542–545, 04 2004.
- <sup>535</sup> [2] 1951 Park, Jong-Hee, 1955 Sudarshan, T. S., and Inc ebrary. Chemical vapor de-  
<sup>536</sup> position. Materials Park, Ohio : ASM International, 2001. Includes bibliographical  
<sup>537</sup> references.
- <sup>538</sup> [3] CIVIDEC Instrumentation GmbH. *sCVD diamond sensor*. <http://www.cividec.at>,  
<sup>539</sup> 2015.
- <sup>540</sup> [4] Heinz Pernegger. *The Pixel Detector of the ATLAS Experiment for LHC Run-2*. Tech-  
<sup>541</sup> nical Report ATL-INDET-PROC-2015-001, CERN, Geneva, Feb 2015.
- <sup>542</sup> [5] Claudia Marcelloni De Oliveira. *IBL installation into the inner detector of the ATLAS*  
<sup>543</sup> *Experiment side C*. General Photo, May 2014.
- <sup>544</sup> [6] *Bremsstrahlung*. 2016.
- <sup>545</sup> [7] Yoshihiko Hatano, Yosuke Katsumura, and A. Mozumder. Charged Particle and Photon  
<sup>546</sup> Interactions with Matter: Recent Advances, Applications, and Interfaces. CRC  
<sup>547</sup> Press, 2010.
- <sup>548</sup> [8] S. Sze and K. N. Kwok. Physics of Semiconductor Devices, 3rd ed. Wiley, Hoboken,  
<sup>549</sup> NJ, 2007.
- <sup>550</sup> [9] W. Blum, W. Riegler, and L. Rolandi. Particle Detection with Drift Chambers, vol-  
<sup>551</sup> ume 2 of *2*. Springer-Verlag, Berlin Heidelberg, 2008.
- <sup>552</sup> [10] W. Shockley. *Currents to Conductors Induced by a Moving Point Charge*. *Journal of*  
<sup>553</sup> *applied Physics*, 9:635, 1938.
- <sup>554</sup> [11] S. Ramo. *Currents Induced by Electron Motion*. *Proceedings of the IRE*, 27:584–585,  
<sup>555</sup> 1939.
- <sup>556</sup> [12] Hendrik Jansen, Norbert Wermes, and Heinz Pernegger. *Chemical Vapour Deposition*  
<sup>557</sup> *Diamond - Charge Carrier Movement at Low Temperatures and Use in Time-Critical*  
<sup>558</sup> *Applications*. PhD thesis, Bonn U., Sep 2013. Presented 10 Dec 2013.

## BIBLIOGRAPHY

---

- [559] [13] Hendrik Jansen, Daniel Dobos, Thomas Eisel, Heinz Pernegger, Vladimir Eremin, and  
560 Norbert Wermes. Temperature dependence of charge carrier mobility in single-crystal  
561 chemical vapour deposition diamond. *Journal of Applied Physics*, 113(17), 2013.
- [562] [14] Z. Li and H. Kraner. *Modeling and simulation of charge collection properties for neutron*  
563 *irradiated silicon detectors. Nuclear Physics B - Proceedings Supplements* 32, (32):398–  
564 409, 1993.
- [565] [15] Peter Sigmund. Particle Penetration and Radiation Effects Volume 2 - General Aspects  
566 and Stopping of Swift Point Charges, volume 151 of *Springer Series in Solid-State*  
567 *Sciences*. Springer-Verlag Berlin Heidelberg, 2006.
- [568] [16] U. Fano. Ionization Yield of Radiations. II. The Fluctuations of the Number of Ions.  
569 *Physical Review*, 72:26–29, July 1947.
- [570] [17] R. C. Alig, S. Bloom, and C. W. Struck. Scattering by ionization and phonon emission  
571 in semiconductors. 22:5565–5582, December 1980.
- [572] [18] Claude A. Klein. Radiation-induced energy levels in silicon. *Journal of Applied Physics*,  
573 30(8):1222–1231, 1959.
- [574] [19] Marco Marinelli, E. Milani, M. E. Morgada, G. Pucella, G. Rodriguez, A. Tuccia-  
575 rone, G. Verona-Rinati, M. Angelone, and M. Pillon. Thermal detrapping analysis of  
576 pumping-related defects in diamond. *Applied Physics Letters*, 83(18):3707–3709, 2003.
- [577] [20] M. Huhtinen. *Simulation of non-ionising energy loss and defect formation in sili-*  
578 *con. Nuclear Instruments and Methods in Physics Research A*, 491:194–215, September  
579 2002.
- [580] [21] Moritz Guthoff, Wim de Boer, and Steffen Mller. Simulation of beam induced lat-  
581 tice defects of diamond detectors using {FLUKA}. *Nuclear Instruments and Methods in Physics*  
582 *Research Section A: Accelerators, Spectrometers, Detectors and Associated Equipment*, 735:223 – 228, 2014.
- [584] [22] Determination of operational dose equivalent quantities for neutrons. ICRU, Wash-  
585 ton, DC, 2001.
- [586] [23] RD42 collaboration. <http://rd42.web.cern.ch/rd42/>.
- [587] [24] M. Mikuž. *Diamond sensors for high energy radiation and particle detection*. TIPP,  
588 2011.
- [589] [25] J. L. Yarnell, J. L. Warren, and R. G. Wenzel. Lattice vibrations in diamond. *Phys.*  
590 *Rev. Lett.*, 13:13–15, Jul 1964.
- [591] [26] W. Y. Liang. Excitons. *Physics Education*, 5:226–228, July 1970.
- [592] [27] J. B. Johnson. *Thermal Agitation of Electricity in Conductors*. *Phys. Rev.*, 32:97–109,  
593 Jul 1928.

## BIBLIOGRAPHY

---

- 594 [28] H. Nyquist. *Thermal Agitation of Electric Charge in Conductors.* *Phys. Rev.*, 32:110–  
595 113, Jul 1928.
- 596 [29] Xilinx Virtex 5 FPGA. <http://www.hdl.co.jp/XCM-109/top.560.jpg>.
- 597 [30] M. Garcia-Sciveres. ATLAS Experiment Pixel Detector Upgrades. 2011.